Materials Today Chemistry 38 (2024) 102133

Contents lists available at ScienceDirect

Materials Today Chemistry

journal homepage: www.journals.elsevier.com/materials-today-chemistry/

Exploring triazene derivative's antimicrobial activity and its incorporation onto 3D-printed coatings

Pedro Vieira [a,b], Ana F. Bettencourt [a], Efthymia Panteli [a,c], Catarina Santos [d,e], Lídia M. Gonçalves [a], Ana P. Francisco [a,**], Isabel A.C. Ribeiro [a,*]

[a] Research Institute for Medicines (iMed.ULisboa), Faculty of Pharmacy, Universidade de Lisboa. Avenida Prof. Gama Pinto, 1649-003, Lisboa, Portugal
[b] Faculdade de Ciências e Tecnologia, Universidade Nova de Lisboa, Campus de Caparica, 1829-516, Caparica, Portugal
[c] Pharmacy Department, National and Kapodistrian University of Athens, 30, Panepistimiou Street, 10679, Athens, Greece
[d] EST, Setúbal CDP2T, Instituto Politécnico de Setúbal, Campus IPS, 2910, Setúbal, Portugal
[e] CQE, Institute of Molecular Sciences, Instituto Superior Técnico, Universidade de Lisboa, Av. Rovisco Pais, 1049-001, Lisboa, Portugal

ARTICLE INFO

Keywords:
1,3-diaryltriazenes
Antimicrobial
Surface coating
Biofilm inhibition
3D-printing
PDMS

ABSTRACT

Antimicrobial resistance has emerged as a significant health concern demanding the urgent development of new active molecules. Furthermore, within healthcare settings, medical devices can be the cause of microorganisms' proliferation leading to infection. Thus, nowadays the need for novel antimicrobial biomaterials is mandatory. In this work different 1,3-diaryltriazenes were synthesized for incorporation as antimicrobials onto 3D-printed hydrogel coatings for polydimethylsiloxane (PDMS) substrates used in the production of different medical devices. Symmetric and asymmetric aryltriazenes were synthesized and characterized by spectroscopic methods. Antimicrobial activity was screened and the most active triazene was selected to be incorporated into the 3D-printed coatings that were further characterized by contact angle measurements, FTIR-ATR, SEM, drug release, antimicrobial activity, and cytocompatibility.

The 1,3-bis (4-nitro-2-(trifluoromethyl)phenyl) triazene showed activity against *Staphylococcus aureus* with a minimum inhibitory concentration of 1 μg/mL and revealed no cytotoxicity towards HaCat cells. 3D-printed hydrogel coatings (comprising chitosan/starch and sodium alginate) loaded triazene were successfully produced for PDMS substrates. Triazene coatings presented high wettability and smoothness and revealed antimicrobial and antibiofilm activity (i.e., 96 % reduction) towards *S. aureus*. Additionally, the produced coatings showed no cytotoxicity under the tested conditions. This study marks the initial proof that incorporating triazenes into 3D-printed hydrogel-based coatings can diminish biofilm formation on widely used biomaterials, such as PDMS surfaces. Herein achieved outcomes have allowed us to confirm and propose a novel type of hybrid construct as an antimicrobial hydrogel coating.

1. Introduction

The continuous rise in microbial resistance has led to an ever-increasing demand for developing new antimicrobials with novel mechanisms of action to fight infections [1,2]. The suggestion of molecules initially intended for a distinct disease that can also be active as antimicrobials, known as drug repurposing, can be a possible strategy [3]. Organic triazene derivatives are an example of active molecules with a very different skeleton and expected new mechanisms of action as antimicrobials. Triazenes are compounds defined by the presence of three consecutive nitrogen atoms, linked by a single and double bond (R''R'-N-N═N–R). Derivatives of these compounds have been investigated for almost 150 years and have shown to possess various biological activities, the most studied being their cytotoxic activity against several types of tumor cells [4]. Currently, there are two antineoplastic agents (dacarbazine and temozolomide) approved by the FDA, which have triazenes as active functionality [5]. Thus, although triazenes are known for their antineoplastic activity the evaluation of this class of molecules as possible antimicrobials can be an interesting strategy to discover new antimicrobial agents. There are exploratory studies about the biological

* Corresponding author. Faculty of Pharmacy, Universidade de Lisboa, Avenida Prof. Gama Pinto, 1649-003, Lisboa, Portugal.
** Corresponding author.
E-mail addresses: afrancis@ff.ulisboa.pt (A.P. Francisco), iribeiro@ff.ulisboa.pt (I.A.C. Ribeiro).

https://doi.org/10.1016/j.mtchem.2024.102133
Received 14 January 2024; Received in revised form 20 May 2024; Accepted 23 May 2024
Available online 30 May 2024

evaluation of triazenes against bacteria, and only in recent years, they have been studied for their potential application as antibacterial agents [6–9]. In these studies, most triazenes evaluated were 1,3-diaryltriazenes (R''R'-N-N═N–R, R, and R' = Ar) and results showed a preference for activity against Gram-positive bacteria. Triazenes can inhibit the proliferation (bacteriostatic effect) or kill these bacteria (bactericidal effect), depending on the substituent in the aromatic ring [7,10]. Interesting biological activities have been achieved against *Mycobacterium tuberculosis*-resistant strains where 1,3-diaryltriazenes carrying a NO_2 group had showed $IC_{50} < 1$ μM [10]. Methicillin-resistant *Staphylococcus aureus* (MRSA) strains have shown susceptibility to the corresponding acyl derivatives of the referred 1,3-diaryltriazenes with MIC values < 1 μM [7].

Along with the lack of novel antimicrobial molecules, several difficult-to-treat infections are medical device-related since most biomaterial surfaces are prone to microbial colonization and thus biofilm formation [11]. Biofilms can be described as an extracellular polymeric matrix produced by microorganisms that increases the chance of their survival by resisting mechanical stresses imposed on these communities and by conferring resistance/tolerance against many antimicrobial agents [12,13]. This brings forward the problem of how to prevent biofilm formation on medical device surfaces. There have been efforts to find new biomaterials, surfaces or coatings to reduce the first attachment of microorganisms and prevent infection [14]. These new surfaces can be distinguished in two ways: coatings that kill bacteria (antimicrobial) and coatings that hinder microbial adherence (antifouling) [14–16]. Every antimicrobial coating comprises a microbe-killing agent. The biocide may function when the microbe comes in touch with it (contact killing) or is released over time [15,16]. These types of coatings can be produced through conventional techniques (spray coating, dipping), but 3D-printing technology is an emerging trend due to the versatility of designs that allow personalized medicine [17,18]. By combining this technique with biocompatible materials, such as natural hydrogel polymers, it is possible to create a porous matrix that may have different uses in the medical field, such as drug release systems [19,20]. Thus, these 3D-printed polymeric matrices can be used to coat biomedical materials (such as polydimethylsiloxane, PDMS) to increase their antimicrobial activity and reduce related infections. Different polysaccharide polymers have been tested as inks for 3D printing. When considering antimicrobial polymers chitosan is generally selected [21] and to improve chitosan's hydrogel printability other components can be added namely starch [22]. Moreover, the antibiofilm activity of a coating will certainly increase if an antimicrobial compound is added to be released through time. In this field, a common delivery system is a sodium alginate hydrogel [23].

The herein present work aimed at synthesizing 1,3-diaryltriazenes derivatives and studying their suitability to be incorporated into a 3D-printed antimicrobial coating. The 1,3-diaryltriazenes derivatives (8 compounds) comprising symmetrical triazenes, and asymmetrical ones containing a sulfathiazole moiety were first screened for their antimicrobial and cytotoxicity activity. The most suitable derivative was selected to be incorporated into a sodium alginate hydrogel and introduced into the pores of a chitosan-starch 3D-printed coating. The surfaces of the coatings were further characterized regarding FTIR-ATR, SEM, and wettability. Finally, coatings suitability was evaluated through triazene release, antimicrobial/antibiofilm activity, and cytocompatibility studies.

2. Materials and methods

2.1. General information

Chemicals used in the synthesis were purchased from Sigma–Aldrich Chemical Company, BDH, Merck Chemical Company, Fluorochem, or Alfa Aeser. All chemicals were of analytical grade. The solvents were obtained from commercial suppliers and further purified by additional destilation with the appropriate desiccant agent.

Melting points were determined in a Köfler camera Bock-Monoscop "M" and are uncorrected.

IR spectra were acquired using Attenuated Total Reflectance Fourier Transform Infrared spectroscopy (ATR-FTIR), using a Nicolet 6700 Thermo Scientific Class 1 Laser Product. Purified compounds were placed on the ATR diamond crystal and spectra were recorded between 4000 and 800 cm^{-1} (128 scans recorded at 8 cm^{-1} resolution).

^{1}H and ^{13}C NMR spectra were recorded in DMSO-d_6 using a Bruker® - Biospin Fourier 300 spectrometer. Chemical shifts, (δ), are reported in parts per million (ppm) relative to the solvent residual peak, multiplicity (s: singlet; d: doublet; t: triplet; dd: doublet of doublets; m: multiplet), and coupling constants (J), in Hz.

Mass spectra were recorded in a Waters Micromass Quattro micro API Benchtop Mass Spectrometer.

2.2. Synthesis of 1,3-diaryltriazenes

Method A- In a round bottom flask, containing a solution of aniline (1.00 mmol) in 5 % aqueous HCl (1.50 mL) at 0 °C, was added dropwise, the aqueous solution of sodium nitrite (1.00 mmol, 68.99 mg/2.00 mL). The mixture was stirred for 1 h at 0 °C to form the respective diazonium salt. To the solution of the diazonium salt were added, sulfathiazole (1 mmol) or the sarting aniline (1 mmol) to form asymmetric (**2a-f**) and symmetric (**3a**) triazenes, respectively. After addition, the reaction mixture was stirred for 20–24 h at room temperature. The formed precipitate was vacuum-filtered and washed with cold water (3 x 10 mL) [24].

The reactions were monitored by thin-layer chromatography (TLC) using Silica Gel 60 F_{254} aluminum plates (Merck, Darmstadt, Germany) and visualized using a CAMAG UV lamp.

Purification of the compounds was done by column chromatography using silica gel 60 (0.040 nm-0.063 nm) or by recrystallization.

Method B - In a round bottom flask containing a solution of aniline (1 mmol) in dichloromethane (DCM) (4.00 mL) at 0 °C, was added a solution of *tert*-butyl nitrite (1.50 mmol, 154 mg, 179 μL) in DCM (4.00 mL). The solution was stirred for 4 h and the solvent evaporated to dryness. The reactions were monitored by TLC using Silica Gel 60 F_{254} aluminum plates (Merck, Darmstadt, Germany) and visualized using a CAMAG UV lamp.

The crude product was purified by preparative TLC (PTLC), using silica gel 60 F_{254} and eluted with (Hexane: Ethyl acetate 80:20 (v/v)).

2.2.1. 4-(3-(4-methoxy-2-nitrophenyl)triaz-1-en-1-yl)-N-(thiazol-2-yl) benzenesulfonamide (2a)

Method **A**; TLC CH_2Cl_2:Methanol (9,5:0,5); column chromatography DCM:MeOH (9,5:0,5). Orange powder; m.p. = 172 °C, yield: 12 %; IR (ATR) ν_{max} (cm^{-1}): 3261 (N–H); 1594 (N–O); 1515 (N═N); 1294 (N–N) 1243 (SO_2); 1137 (SO_2); 929 (S–N thiazole); ^{1}H NMR (300 MHz, DMSO-d_6) δ (ppm): 13.99 (s, 1H, NH), 12.67 (s, 1H, NH), 7.50 (d, J = 2.8 Hz, 1H, Ar-CH); 7.32–7.20 (m, 2H, Ar-CH); 7.83–7.70 (m, 3H, Ar-CH); 7.43 (d, J = 8.5 Hz, 2H, Ar-CH); 6.81 (d, J = 4.8 Hz, 1H, thiazole); 7.32–7.20 (d, J = 4.8, 1H, thiazole); 3.86 (s, 3H, OMe); ^{13}C NMR (75 MHz, DMSO-d_6) δ (ppm): 169.1 (S–C═N, thiazole), 146.7 (C–N═N triazene), 144.6 (Ar-C-O), 136.4 (Ar-C-NO_2), 128.1 (N–*CH*═C thiazole), 124.8 (Ar-C-S), 121.1 (Ar-CH), 119.6 (Ar-CH), 114.5 (Ar-CH), 108.5 (Ar-CH), 108.3 (S–*CH*═C thiazole), 56.7 (OMe); MS (ESI+) m/z $[M+H]^+$ 435.57.

2.2.2. 4-(3-(2-nitrophenyl)triaz-1-en-1-yl)-N-(thiazol-2-yl) benzenesulfonamide (2b)

Method **A;** TLC CH_2Cl_2: Methanol (9,5:0,5); column chromatography DCM:MeOH (9,5:0,5). Yellow solid; m.p. = 178–179 °C, yield: 35 %; IR (ATR) ν_{max} (cm^{-1}):3417 (N–H) 3311 (N–H); 1569 (N–O); 1527 (N═N); 1338 (NO_2); 1294 (SO_2); 1137 (SO_2); 937 (S–N); ^{1}H NMR (300 MHz, DMSO-d_6) δ (ppm): 13.27 (s, 1H, NH), 12.75 (s, 1H), 7.89 (d, J = 8.1 Hz,

1H, Ar-CH), 7.85–7.66 (m, 4H, Ar-CH), 7.55–7.41 (m, 3H, Ar-CH), 7.24 (d, $J = 4.8$ Hz, 1H, thiazole), 6.82 (d, $J = 4.8$ Hz, 1H, thiazole); ^{13}C NMR (75 MHz, DMSO-d_6) δ (ppm): 169.1 (S–C═N, thiazole), 145.9 (Ar-C-N═N triazene), 144.3 (Ar-C-N-N), 142.1(Ar-C-NO_2), 137.0 (N–*CH*═C thiazole), 133.3 (Ar-C-S), 128.1 (Ar-CH), 124.9 (Ar-CH), 124.0 (Ar-CH), 120.3 (Ar-CH), 114.8 (Ar-CH), 108.6 (S–*CH*═C thiazole); MS (ESI+) *m/z* $[M+H]^+$ 405.62.

2.2.3. 4-(3-(4-nitrophenyl)triaz-1-en-1-yl)-N-(thiazol-2-yl) benzenesulfonamide (2c)

Method **A;** TLC CH_2Cl_2:Methanol (9,5:0,5); recrystallized from ethanol. Orange powder; m.p. = 199–201 °C, yield: 19 %; IR (ATR) ν_{max} (cm^{-1}): 3293 (N–H) 1598 (C═N); 1502 (N═N); 1324 (N–O); 1238 (SO_2); 1137 (SO_2); 937 (S–N); ^{1}H NMR (300 MHz, DMSO-d_6) δ (ppm): 13.23 (s, 1H, NH), 12.69 (s, 1H, N–H), 8.27 (d, $J = 9.2$ Hz, 2H, Ar-CH), 7.86 (d, $J = 8.2$ Hz, 2H, Ar-CH), 7.70 (m, 2H, Ar-CH), 7.55 (m, 2H, Ar-CH), 7.26 (d, $J = 4.8$ Hz, 1H, thiazole), 6.84 (d, $J = 4.8$ Hz, 1H, thiazole); ^{13}C NMR (75 MHz, DMSO-d_6) δ (ppm): 169.3 (S–C═N, thiazole), 152.9 (Ar-C-N═N triazene), 147.6 (Ar-C-NO_2), 142.5 (Ar-C-N-N), 141.5 (N–*CH*═C thiazole) 127.7 (Ar-C-S), 126.2 (Ar-CH), 124.9 (Ar-CH), 122.1 (Ar-CH), 114.6 (Ar-CH), 108.8 (S–*CH*═C thiazole); MS (ESI+) *m/z*$[M+H]^+$ 405.71.

2.2.4. 4-(3-(4-nitro-2-(trifluoromethyl) phenyl) triaz-1-en-1-yl)-N-(thiazol-2-yl) benzenesulfonamide (2d)

Method A; TLC CH_2Cl_2: Methanol (9,5:0,5); recrystallized from ethanol. Yellow powder, m.p. = 210–212 °C, yield: 14 %; IR(ATR) ν_{max} (cm^{-1}): 3293 (N–H); 1598 (C═N); 1502 (N–O); 1324 (N–O); 1238 (SO_2); 1137 (SO_2); 937 (S–N); ^{1}H NMR (300 MHz, DMSO-d_6) δ (ppm): 13.27 (broad, NH), 8.53–8.45 (m, 2H, Ar-CH), 8.05 (d, $J = 8.7$ Hz, 1H, Ar-CH), 7.84 (d, $J = 8.7$ Hz, 2H, Ar-CH, 7.60 (d, $J = 8.7$ Hz, 2H, Ar-CH), 7.25 (d, $J = 4.8$ Hz, 1H, thiazole), 6.83 (d, $J = 4.8$ Hz, 1H, thiazole); ^{13}C NMR (75 MHz, DMSO-d_6) δ (ppm): 169.2 (S–C═N, thiazole), 152.6 (Ar-C-N═N triazene), 145.2 (Ar-C-N-N), 143.9 (Ar-C-NO_2), 138.0 (N–*CH*═C thiazole), 128.9 (Ar-C-S), 128.1 (Ar-CH), 124.9 (Ar-CH), 122.8 (CF_3), 120.4 (Ar-CH), 115.8 (Ar-C-CF_3), 108.6 (S–*CH*═C thiazole); MS (ESI+) *m/z* $[M+H]^+$ 473.58.

2.2.5. 4-(3-(4-nitro-3-(trifluoromethyl) phenyl) triaz-1-en-1-yl)-N-(thiazol-2-yl)benzenesulfonamide (2e)

Method A; TLC CH_2Cl_2: Methanol (9,5:0,5); recrystallized from ethanol. Orange poder, m.p. = 197–199 °C, yield: 13 %; IR (ATR) ν_{max} (cm^{-1}): 3480 (N–H); 1598 (C═N); 1517 (N–O); 1249 (SO_2); 1132 (SO_2); 931 (S–N); ^{1}H NMR (300 MHz, DMSO-d_6) δ (ppm): 13.37 (s, 1H, NH), 12.76 (s, 1H, NH), 8.24 (d, $J = 9.3$ Hz, 1H, Ar-CH), 7.96–7.77 (m, 4H, Ar-CH), 7.73 (s, 2H, Ar-CH), 7.26 (d, $J = 4.8$ Hz, 1H, thiazole), 6.84 (d, $J = 4.8$ Hz, 1H, thiazole); ^{13}C NMR (75 MHz, DMSO-d_6) δ (ppm): 169.3 (S–C═N, thiazole), 142.0 (Ar-C-N═N triazene), 141.4 (Ar-C-N-N). 128.9 (Ar-CH), 127.7 (Ar-CH), 124.9 (Ar-CH), 124.2 (Ar-CH), 120.6 (CF_3), 108.7 (S–*CH*═C thiazole); MS (ESI+) *m/z* $[M+H]^+$ 473.55.

2.2.6. 4-(3-(2-fluoro-4-nitrophenyl) triaz-1-en-1-yl)-N-(thiazol-2-yl) benzenesulfonamide (2f)

Method A; TLC CH_2Cl_2: Methanol (9,5:0,5); recrystallized from ethanol. Orange powder; m.p. = 184–186 °C yield: 12 %; IR (ATR) ν_{max} (cm^{-1}): 3212 (N–H); 1596 (C═N); 1510 (N–O); 1330 (N–O); 1255 (SO_2); 1137 (SO_2); 935 (S–N); ^{1}H NMR (300 MHz, DMSO-d_6) δ (ppm): 13.63 (s, 1H, N–H), 12.73 (s, 1H, N–H), 8.23 (dd, $J = 8.7$, 2.5 Hz, 1H, Ar-CH), 8.12 (dd, $J = 9.1$, 2.5 Hz, 1H, Ar-CH), 7.93 (t, $J = 8.4$ Hz, 1H, Ar-CH), 7.84 (d, $J = 8.3$ Hz, 2H, Ar-CH), 7.56 (s, 2H, Ar-CH), 7.25 (d, $J = 4.8$ Hz, 1H, thiazole), 6.83 (d, $J = 4.8$ Hz, 1H, thiazole); ^{13}C NMR (75 MHz, DMSO-d_6) δ (ppm): 169.2(S–C═N, thiazole), 146.1 (Ar-C-N═N triazene), 143.8 (Ar-C-N-N), 128.1 (Ar-CH), 124.9 (Ar-CH), 113.4 (Ar-CH), 113.1 (Ar-C-F), 108.7 (S–*CH*═C thiazole); MS (ESI+) *m/z* $[M+H]^+$ 423.5.

2.2.7. 1,3-bis(4-nitro-2-(trifluoromethyl)phenyl) triazene (3a)

Method **A;** TLC hexane:ethyl acetate (7:3); Recrystallized from ethanol/water. Pale yellow powder; yellow in DCM solution and violet in acetone and ethanol solutions; m.p = 187-188 °C, yield: 40 %. IR (ATR) ν_{max} (cm^{-1}): 3330 (NH); 1592 (N–O); 1510 (N═N); 1330 (N–O); 1261 (N–N); 1251 (CF_3); ^{1}H NMR (300 MHz, DMSO-d_6) δ (ppm): 13.68 (s, 1H, NH), 8.56 (dd, $J = 8.9$ Hz, $J = 2.7$ Hz 2H, Ar-CH), 8.52 (d, J = 2.7, 2H, Ar-CH), 7.94 (d, $J = 8.9$ Hz, 2H, Ar-CH). ^{13}C NMR (75 MHz, DMSO-d_6) δ (ppm): 147.9 (N═N–C), 144.8 (C–NO_2), 129.2 (Ar-CH), 124.9 (CF_3), 123.6 (Ar-CH), 123.5 (Ar-C-CF_3), 121.3 (Ar-CH); MS (ESI+) *m/z* $[M+H]^+$ 423.60.

2.2.8. 1,3-bis(4-methoxy-2-nitrophenyl) triazene (3b)

Method **B**; TLC hexane:ethyl acetate (9:1); Red oil; yield: 20 %; IR (ATR) ν_{max} (cm^{-1}): 3309 (N–H); 1521 (N–O); 1348 (N–O); 1247 (N–N); 1031 (C–*O*–C); ^{1}H NMR (300 MHz, DMSO-d_6) δ (ppm): 12.26 (s, 1H, NH), 7.83 (dd, $J = 8.1$, 0.9 Hz, 1H, Ar-CH), 7.71 (t, $J = 2.4$ Hz, 1H, Ar-CH), 7.58 (t, J = 8.1, 1H, Ar-CH), 7.42 (dd, J = 8.1, 2.4, 2H, Ar-CH), 7.37 (d, $J = 3.0$ Hz, 1H, Ar-CH), 3.88 (s, 6H, MeO); MS (ESI+) *m/z* $[M+H]^+$ 348.37.

2.3. Screening of active compounds

2.3.1. Antimicrobial activity

2.3.1.1. Microorganisms and growth conditions. *Staphylococcus aureus* ATCC 25923, *Escherichia coli* ATCC 25922, *Pseudomonas aeruginosa* NCTC 12903, *Enterococcus faecalis* NCTC 12697, *Proteus mirabilis* NCTC 13376, and *Candida albicans* ATCC 10231 were obtained from the American Type Culture Collection (ATCC) or the National Collection of Type Cultures (NCTC). Aliquots from frozen stocks at −80 °C were used to culture microorganisms on tryptic soy agar (TSA, Biokar Diagnostics) or Sabouraud dextrose agar (SDA, Biokar Diagnostics) for bacteria and yeast, respectively, for 24 h at 36 °C.

2.3.1.2. Planktonic cells susceptibility assays. With bacteria the minimum inhibitory concentration (MIC) of each synthesized compound was accessed in Mueller-Hinton (MH) medium (Biokar, Beauvais, France) by the microdilution broth method [25,26] with a few modifications. Briefly, different stock dilutions of each compound were performed in DMSO (Merck, Darmstadt, Germany) with concentrations ranging from 12.8 to 0.25 mg/mL. The MIC experiments were carried out in a 96-well microtiter plate (MTP) and 2 μL of the previous dilutions [27] were added to each well to reach final test concentrations ranging from 128 to 0.25 μg/mL. A levofloxacin standard solution was serially 2-fold diluted to achieve concentrations ranging from 16.0 μg/mL to 0.03 μg/mL, in sterile MH broth, for assay control. As a negative control, 200 μL of Mueller Hinton broth were added to a row and as a positive control, a row of wells with MH broth was inoculated with the testing bacteria. To prepare the inoculum colonies from 24-h cultures were suspended in MH broth and the inoculum was further adjusted to reach 0.5 McFarland units (Biochrom, Ultrospec 10-cell density meter). In each well of the 96-well MTP the final inoculum concentration was 5×10^5 CFU/mL, plates were incubated (VWR INCU-Line 150R incubator) under static conditions for 24 h at 36 °C and results were assessed. Additionally, to obtain the minimum bactericidal concentration (MBC) for the tested compounds, wells with no bacterial growth on MIC assay were further tested. From the plates used for testing the MIC, 20 μL of each well without visible growth was transferred onto 180 μL of MH broth, plates were incubated at 36 °C for 24 h, and results were assessed.

The same procedure was performed in MIC assay with *Candida albicans* and the experiments were carried out with RPMI 1640 medium buffered with MOPS (Thermo Fisher Scientific, Massachusetts, USA) [28]. As assay control fluconazole was serially 2-fold diluted into concentrations ranging from 16 to 0.03 μg/mL. Negative and positive

controls were also performed in RPMI medium buffered with MOPS. The inoculum was prepared in RPMI 1640 broth buffered with MOPS and the final inoculum concentration in each well was 5×10^3 CFU/mL. The plate was then incubated (VWR INCU-Line 150R incubator) at 36 °C for 24 h and results were assessed.

2.3.2. In vitro cytocompatibility

The cytotoxicity was assessed using Alamar Blue (resazurin, 7-Hydroxy-3H-phenoxazin-3-one 10-oxide) (Applichem, Darmstadt; Germany) and MTT (3-(4,5- dimethylthiazol-2-yl)-2,5-diphenyltetrazolium bromide) (Applichem, Darmstadt; Germany) as metabolic endpoints and propidium iodide (PI) dye (Applichem, Darmstadt; Germany) exclusion as membrane integrity assay [29]. Briefly, the day before the experiment HaCaT cells, a spontaneously immortalized human keratinocyte cell line (CLS, Germany), were seeded in 96 well tissue culture plates at a cell density of $2x10^4$ cells per well, in RPMI 1640 culture medium (Gibco, Thermo Fisher Scientific Inc. Paisley; Scotland) supplemented with 10 % Fetal serum bovine (Gibco, Thermo Fisher Scientific Inc. Paisley; Scotland), 100 unit/mLs of penicillin G (sodium salt) (Gibco, Thermo Fisher Scientific Inc. Paisley; Scotland), 100 μg/mL of streptomycin sulfate (Gibco, Thermo Fisher Scientific Inc. Paisley; Scotland) and 2 mM L-glutamine (Gibco, Thermo Fisher Scientific Inc. Paisley; Scotland) and incubated at 37 °C and 5 % CO_2 in a humidified atmosphere. Cells were incubated with the test solution of compound **3a** (100, 50, 25, 12.5, and 6.25 μM), culture medium, and 1 mg/mL of sodium dodecyl sulfate (SDS) (Applichem, Darmstadt; Germany) as negative and positive controls, respectively. After 24 h of exposition medium was replaced by 0.3 mM PI in the culture medium. Fluorescence was measured (excitation, 485 nm; emission, 590 nm) in a Microplate Reader (FLUOstar Omega, BMGLabtech, Germany), and then the Alamar Blue and MTT assay were performed. The medium was replaced by a medium containing 5.0 mM of resazurin. After 3 h of incubation, the fluorescence was measured (excitation, 530 nm: emission, 590 nm) in a Microplate Reader (FLUOstar Omega, BMGLabtech, Germany). For the MTT assay, the medium was replaced with medium containing 0.5 mg/mL of MTT, and after 3 h of incubation the MTT was extracted with DMSO, and the absorbance was measured at 570 nm in a Microplate Reader (FLUOstar Omega, BMGLabtech, Germany).

For the resazurin assay, the relative cell viability (%) compared to control cells was calculated as $\frac{[\text{Fluorescence}]\text{sample}}{[\text{Fluorescence}]\text{control}} \times 100$.

For the MTT assay, the relative cell viability (%) compared to control cells was calculated as $\frac{[\text{Absorbance}]\text{sample}}{[\text{Absorbance}]\text{control}} \times 100$.

The PI uptake ratio was determined as $\frac{[\text{Fluorescence}]\text{sample}}{[\text{Fluorescence}]\text{control}}$.

2.4. 3D-printing of triazene coatings

2.4.1. Preparation of a chitosan-starch hydrogel

A chitosan-starch hydrogel was produced according to Cardoso et al. [22]. Firstly, a 3 % (w/v) chitosan in acetic acid 1 % (v/v) aqueous solution was stirred for 4 h at 800 rpm (VELP Arex-6 Digital Pro) at room temperature and a 78 % (w/v) starch aqueous solution was stirred for 4 h at 800 rpm (VELP Arex-6 Digital Pro) at 95 °C. Then, both solutions were combined and stirred for 3 h at 800 rpm (VELP Arex-6 Digital Pro) at 80 °C to reach a final hydrogel concentration of 2.5 % and 13 % (w/v) of chitosan and starch, respectively. The obtained hydrogel was kept at 4 °C until further usage as ink.

2.4.2. Preparation of sodium alginate-compound 3a hydrogel

Firstly, an ethanolic solution of compound **3a** (8.0 mg/mL) was prepared. Then, 0.2 g of sodium alginate (SA) were added of 1 mL of the ethanolic solution of compound **3a** as well as 4 mL of ultra-purified water. This solution was then stirred at 800 rpm (VELP Arex-6 Digital Pro) at 65 °C for 30 min. The obtained hydrogel presented a concentration of compound **3a** of 2 mg/mL and was kept at 4 °C until further usage.

2.4.3. 3D-printing of the antimicrobial coating

A 3D printer (Regemat 3D bioprinter, BIO V1, Spain) was used to coat medical-grade PDMS segments according to Narciso et al. [26]. The main part of the coating consisted of a 3D-printed porous structure composed of chitosan-starch hydrogel. Thus, firstly, square-shaped 20 × 20 mm coatings with pore sizes of 1.5 × 1.5 mm and a layer height of 0.25 mm were printed, under a flow speed of 0.6 mm/s, on the top medical-grade PDMS. The pores were then filled with alginate-compound **3a** hydrogel extruded from a different syringe of the 3D-printer (0.5 μL per layer). Control coatings with the pores filled with alginate hydrogel free of compound **3a** were also produced. Obtained samples were left to dry for 48 h at 25 °C (VWR INCU-Line 150R incubator).

2.5. Coatings characterization

2.5.1. Surface wettability

Contact angle measurements were carried out with the sessile drop method [26]. Ultra-purified (Milli-Q) water drops (2 μL) were deposited on the surface of dried coatings and images were captured with a digital microscope (Rohs Usb Digital Microscope) connected to a computer. Contact angles were evaluated by image analysis using the Image J software, 5 min after drop deposition. All measurements were performed at room temperature (22 °C) and experiments were evaluated at least in two independent assays with 4 replicates.

2.5.2. FTIR-ATR

Coatings were analyzed by FTIR-ATR according to section 2.1.

2.5.3. SEM

Topographical and morphological evaluation of the 3D-printed chitosan-starch coatings was performed by scanning electron microscopy (SEM) (PhenomProX G6). The X-ray energy dispersive spectrometer (EDS) was used to assess the elemental chemical composition. The conductivity of the samples was improved with a thin coating of conductive gold/palladium (Polaron E−5100). Topographical reconstruction of the 3D-printed chitosan-starch 3D coatings and quantification of the surface roughness parameters were possible through SEM 3D top view image analysis using Thermo Scientific TM 3D Roughness Reconstruction software. The roughness parameters most relevant to the morphological surface texture were graphically displayed.

2.5.4. Release assay

Triazene release from the coatings was accessed according to the previously described methodology [30]. Coatings with triazene-free filling were used as controls. Briefly, the coatings presenting 10 × 10 mm^2 dimensions were fixed on 24-well microtiter plates and subsequently, 2 mL of an isotonic physiological saline solution (NaCl 0.9 wt%; pH 7.4) was added to each well. The plate was incubated at 37 °C (VWR INCU-Line 150R incubator) and shaken at 200 rpm (mini plus IKA, shaker). Samples were collected at pre-determined time points (0.25, 0.5, 2, 4, 5, 6, 24, 48, 72, 168 h) and analyzed for triazene content by UV–vis spectrophotometry at 405 nm (multiplate reader Anthos Zenyth 3100). The amount of triazene in the samples was determined from the standard calibration curve prepared in the concentration range of 2.5–40 μg/mL.

2.6. Antimicrobial activity of coatings

2.6.1. Antibacterial activity

The antimicrobial activity of the coatings was evaluated through the Kirby-Bauer diffusion test towards *S. aureus* ATCC 25923 [31,32]. The inoculum was prepared from 24 h-cultured plates by direct colony suspension in MH broth plates and adjusted to 0.5 McFarland units

(Biochrom, Ultrospec 10-cell density meter). After swabbing the inoculum onto Mueller-Hintor Agar (MHA), 3D-printed coatings, with and without compound **3a**, were placed on top of the solid media. Paper disks with 5 μg of levofloxacin were used as the positive control. Plates were incubated for 24 h at 36 °C and inhibition zones were measured using a Vernier caliper (Mitutoyo Digimatic, MFG.Co., Ltd). Assays were performed in three independent experiments.

2.6.2. Antibiofilm activity

Coated and not coated PDMS segments (10 × 10 mm^2) were fixed to the bottom of the wells of a 24-well MTP. To prepare the inoculum colonies from an *S. aureus* 24-h culture were suspended in BHI medium (Biokar, Beauvais, France) supplemented with 1 % (w/v) glucose and adjusted to a final assay concentration of 1 × 10^6 CFU/mL. The assay was also performed with non-inoculated medium to obtain control samples for each type of coating used. The 24-well MTPs were then incubated (VWR INCU-Line 150R incubator) at 36 °C for 24 h. After 24 h the culture medium was removed, and the wells were twice washed with PBS. Then, biofilm quantification was assessed through the crystal violet assay [25]. Biofilm was first fixed with ethanol (100 %) and further stained with a 0.1 % crystal violet solution (w/v). After 10 min the dye was removed, and the wells were 3 times washed with distilled water. PDMS segments were collected onto 2 mL tubes and 1 mL of 1 % (v/v) acetic acid ethanolic solution was added to each tube and vortexed. Then, 200 μL of each solution was transferred to a 96-well MTP, and the absorbance was measured at 595 nm (Anthos, Zenyth 3100). The biofilm quantification was obtained as: $\frac{[\text{Absorbance}]_{\text{sample}}}{[\text{Absorbance}]_{\text{control}}} \times 100$.

2.7. Cytocompatibility of coatings

The cytocompatibility was assessed with HaCat cells using MTT and propidium iodide (PI) dye exclusion. To the coating samples were added 1 mL of culture medium (RPMI 1640 culture medium supplemented with 10 % Fetal serum bovine, 100 units/mL of penicillin G (sodium salt), 100 μg/mL of streptomycin sulfate and 2 mM L-glutamine) and incubated at 37 °C. Samples of medium were collected after 24 h, 48 h, and 72 h, and cytotoxicity towards HaCaT cells was evaluated after 24 h of contact. The PI and MTT assay were performed as described in the previous section (2.3.2.). For each surface, 6 replicates were analyzed [25,33,34].

3. Results and discussion

3.1. Chemistry

In this work, were synthesized 8 different 1,3-diaryltriazenes according to the synthetic route summarized in Fig. 1. The triazenes were prepared from the reaction of the appropriate aniline precursors with a source of nitrite (*tert*-butyl nitrite for compound **3b** and sodium nitrite for compounds **3a, 2a**– **f**) to form the aryldiazonium salts. To synthesize compounds the formed aryldiazonium salts are coupled with sulfathiazole, for compounds **2a** – **f** or the starting aniline for compounds **3a** and **3b**. Sulfathiazole already presents antimicrobial activity by itself and introducing it to the triazene could amplify its antimicrobial activity.

Compounds **3a-b** were characterized by spectroscopic methods including mono and bidimensional NMR experiments (^{1}H, ^{13}C, HSQC, HMBC), IR (ATR), and mass spectrometry. Analysis of IR spectra confirms the presence of a band corresponding to the N–H stretch of triazene in the range of 3300-3330 cm^{-1}. Other important characteristic bands are the ones from the aromatic nitro group at 1502-1527 cm^{-1} identified as the N–O asymmetric stretching vibrations and at 1315-1348 cm^{-1} corresponding to N–O symmetric vibrations.

Despite the similar structure of **3a** and **3b** the resulting ^{1}H NMR spectra were very different (Fig. 2A an B). A possible explanation for this is the existence of an intramolecular hydrogen bond in compound **3b** that changes the tautomerization rate and makes the signals of the two phenyl rings A and B not equivalent. With compound **3a** the formation of this intramolecular hydrogen bond is not possible and signals from rings A and B are equivalent (Fig. 2B).

Also, this equilibrium occurs at higher rates in the triazenes with lower basicity. Compound **3a** has two electron-withdrawing groups at the *para* (NO_2) and *ortho* (CF_3) positions, which diminish the electron density of the triazene, which in turn, lowers the basicity. On the opposite compound **3b** has an electron-donating group, at the *para* position that increases electron density and basicity. The lower rate of tautomerization in compound **3b** enables the visualization of all the different proton signals in the ^{1}H NMR spectrum.

The analysis of ^{1}H NMR spectra of these compounds allowed the

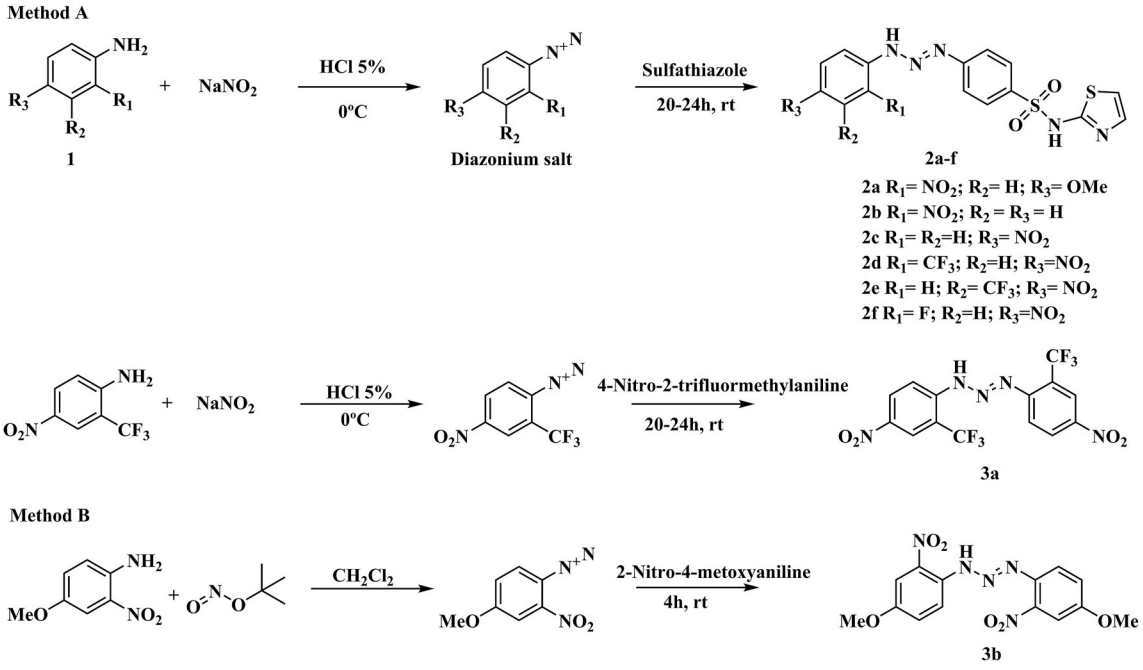

Fig. 1. General synthetic procedures for the synthesis of aryltriazenes **2a-f** (method A) and **3a-b** (method A and B respectively).

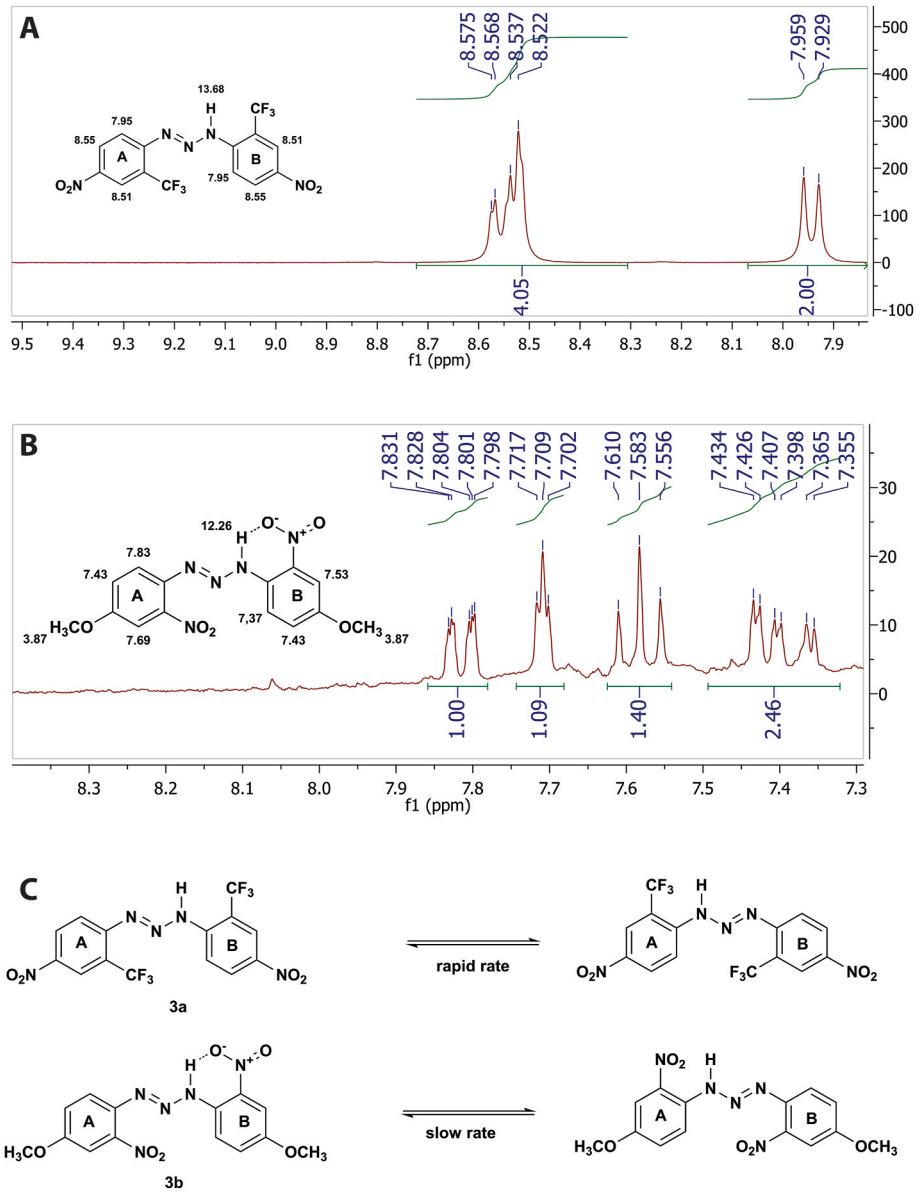

Fig. 2. ^{1}H NMR spectra (A, B) and tautomeric structures (C) of **3a-b** di-substituted 1,3-diaryltriazenes.

identification of the characteristic signal of the triazene NH with chemical shifts >12 ppm. Along with this peak, only aromatic protons were observed between 7.29 and 8.56 ppm for compound **3a**. Compound **3b** presents an additional peak at 3.86 ppm corresponding to the methoxy group as expected.

The asymmetrical 1,3-diaryltriazenes **2a-f** have more complex structures, with the addition of the sulfathiazole group. IR spectra showed the N–H stretch of sulfonamide near 3480 cm^{-1} in addition to the stretch of N–H of the triazene at 3312-3330 cm^{-1}. Additional characteristic bands are: C═N stretch from thiazole ring at 1569-1598 cm^{-1}; the asymmetrical vibration of SO_2 at 1238-1294 cm^{-1}; the symmetrical vibration of SO_2 at 1132-1137 cm^{-1} and the stretch of S–N bond at 929–941 cm^{-1}.

The ^{1}H NMR spectrum of 1,3-diaryltriazenes **2a-f** presented the peaks due to the sulfathiazole moiety. The thiazole ring has two protons with chemical shifts at 6.81–6.84 ppm and 7.18–7.32 ppm as a doublet. Also, the aromatic protons from the six-membered ring appeared around 7.20 ppm and 8.53 ppm.

Regarding ^{13}C NMR analysis of 1,3-diaryltriazenes **2a-f**, the most deshielded peak is the quaternary carbon of the thiazole ring at ~169 ppm. All the carbon atoms from the thiazole ring have chemical shifts quite constants within the series with the other two at ~124 and ~108 ppm. The second most deshielded peak is the signal of the aromatic carbon directly connected to the triazene group, at ~145 ppm. Other peaks in the spectra are consistent with the chemical structures.

3.2. Antimicrobial activity screening

The antimicrobial activity of the compounds **2a-f, 3a, 3b** was tested in concentrations ranging from 128 to 0.25 μg/mL, against different Gram-negative bacteria (*E. coli, P. aeruginosa, P. mirabilis*), Gram-positive bacteria (*S. aureus, E. faecalis*) and yeast (*C. albicans*). The results can be observed in Table 1 as well as MIC values for the controls levofloxacin and fluconazole.

After the incubation period, compound **3a** was the only one able to inhibit growth and kill Gram-positive bacteria. Levofloxacin showed MIC values of 0.25 μg/mL for *S. aureus* and 0.5 μg/mL for *E. faecalis* which is in accordance with the literature validating the MIC assay for compound **3a** [35,36]. Compound **3a** showed a MIC and MBC of 1 μg/mL and 2 μg/mL, respectively, for *S. aureus* and MIC of 4 μg/mL for

Table 1
Screening of compounds **2a-f, 3a, 3b,** Minimal Inhibitory Concentration (MIC) and Minimal Bactericidal Concentration (MBC). The assay was performed with concentrations ranging from 128 to 0.250 μg/mL of triazenes. Levofloxacin and fluconazole concentrations ranged from 16.0 to 0.0312 μg/mL.

Compound	E. faecalis		S. aureus		E. coli		P. mirabilis		P. aureginosa		C. albicans	
	MIC	MBC	MIC	MBC	MIC	MBC	MIC	MBC	MIC	MBC	MIC	MBC
2a	>128	–	>128	–	>128	–	>128	–	>128	–	>128	–
2b	>128	–	>128	–	>128	–	>128	–	>128	–	>128	–
2c	>128	–	>128	–	>128	–	>128	–	>128	–	>128	–
2d	>128	–	>128	–	>128	–	>128	–	>128	–	>128	–
2e	>128	–	>128	–	>128	–	>128	–	>128	–	>128	–
2f	>128	–	>128	–	>128	–	>128	–	>128	–	>128	–
3a	4	>128	1	2	>128	–	>128	–	>128	–	>128	–
3b	>128	–	>128	–	>128	–	>128	–	>128	–	>128	–
Levofloxacin	0.5	–	0.25	–	0.06	–	0.25	–	0.5	–	–	–
Fluconazole	–	–	–	–	–	–	–	–	–	–	0.25	–

E. faecalis. Compound **3a** was not able to kill *E. faecalis* but stopped its growth. In Vajs and colleagues' work MIC of different triazene derivatives ranged between 0.02 and >128 μg/mL depending on the *S. aureus* methicillin-resistant strain used [7]. For Gram-negative bacteria and *C. albicans*, no compound showed activity, suggesting that this class of compounds is not able to penetrate through the cell walls of the yeast and the outer membrane of Gram-negative bacteria or the efflux rate is too high, not allowing for the desired effect. This was studied by Vajs and coworkers [7] when testing triazene derivatives against an *E. coli* with a permeable membrane or without an efflux pump. Those results showed that the triazene derivatives only exhibited activity against the *E. coli* strain with a permeable membrane, revealing that the probable cause for the absence of activity is the inability to penetrate the outer membrane [7].

3.3. In vitro cytocompatibility

Compound **3a** showed the best antibacterial activity under the tested conditions, thus it was selected to be further screened for cytotoxicity (Fig. 3).

The results of PI dye exclusion showed (Fig. 3A) that compound **3a** did not interfere with the cell membrane integrity of HaCaT cells in all concentrations tested after 24 h of exposure. The results of the ratio of PI uptake (Fig. 3A) were not different from cells in the culture medium (negative control) but were different from cells exposed to SDS (positive control).

After assessing the membrane integrity, the cytotoxicity of the compound was tested by performing Alamar blue and MTT assays (Fig. 3B and C, respectively) [37]. In both tests, compound **3a** showed no cytotoxicity effects on HaCaT cells after 24 h of exposure in the range of concentrations tested (6.25–100 μM corresponding to 2.65–42.3 μg/mL). Cell viability assays had already been performed with sodium salt of compound **3a** against primary normal human keratinocyte cells using an MTT test. Results showed that at 25 μg/mL viability was approximately 30 % [7]. The increased cytotoxic activity showed by the sodium salt of compound **3a** could be explained by the different susceptibility of the different cell lines used in the assays and/or by the different solubility profiles of both compounds (neutral and sodium salt).

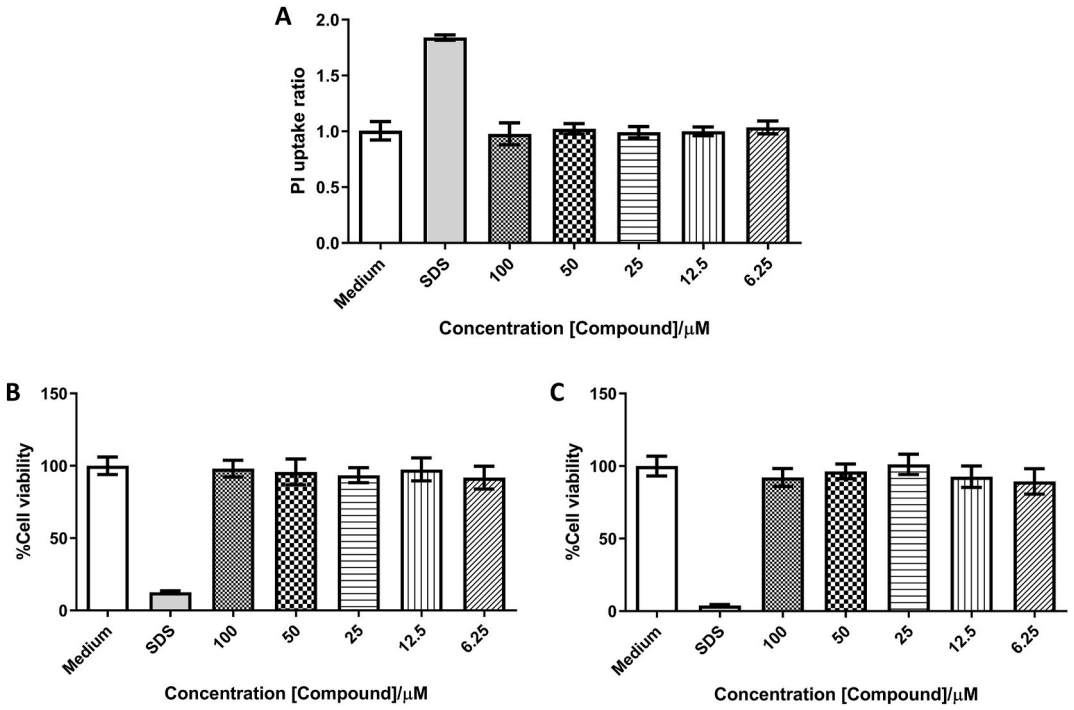

Fig. 3. Cytocompatibility of HaCaT cells after 24 h of exposition time **A.** Ratio of PI uptake (mean ± SD, n = 4). **B.** Relative cell viability determined by the resazurin reduction (mean ± SD, n = 7). **C.** Relative cell viability was determined by the MTT reduction (mean ± SD, n = 7).

3.4. 3D-printed coatings

The sodium alginate (SA) gel incorporating compound **3a** resulted in a yellow gel. The SA was used because of its biocompatibility as well as its suitability as a drug-release polymer [23]. The addition of a 78 % starch solution to a 3 % chitosan solution resulted in a milky white gel, with suitable printing viscosity. For printing an extrusion-based method featured in a 3D bioprinter was used by loading the gels into the syringes attached to the printer. A design software (Regemat 3D Designer, Spain) was used to create the model of the coating. The parameters used were selected in accordance with Cardoso and coworkers [22] since they optimized 3D printing for chitosan-starch-based scaffolds. An example of the obtained coatings is presented in Fig. 4A.

3.5. Coatings characterization

To assess the surface wettability of the produced coatings, contact angles of Milli-Q water were measured on the surface of drug-free coating designated as a blank coating (B-coat) and alginate-compound **3a** coating designated as triazene coating (Tz-coat) (Fig. 4B). The results obtained showed that after stabilization the Tz-coat showed higher wettability (33.68° ± 2.78°), as well as the B-coat (50.98 ± 6.91°) when compared to pristine PDMS (70.61 ± 3.15°). This may be advantageous since it may help prevent the adhesion to hydrophobic surfaces associated with some microorganisms, such as *S. aureus,* and of other fouling agents that could decrease the efficiency of the coating [25]. Films of alginate and chitosan have revealed values of 32.28° ± 0.2 and 63.19 ± 0.03°, respectively [38].

The FTIR-ATR spectra of the individual compounds and the produced coatings are shown in Fig. 4C_1 and 4C_2, respectively. PDMS spectra showed characteristic bands, namely, the symmetric vibration of the bond Si–*O*–Si at 792 cm^{-1} and symmetric vibration at 1008 cm^{-1}. Besides these two, there was also the band at 1259 corresponding to the bond Si–CH_3 [39]. For chitosan, characteristic absorption bands were observed, such as: the broad band of vibration of the hydroxyl groups at 3330 cm^{-1}, the stretching vibrations of the C–H bonds at 2964 cm^{-1}, the N–H bending from amine at 1546 cm^{-1}, the –CH_2 bending at 1405 cm^{-1} and the skeletal vibration of C–O (glycoside bond) stretching at 1002 cm^{-1} [40,41]. In the spectrum of starch, it was possible to identify the OH stretching at the broad band at 3330 cm^{-1} and the stretching vibration of the C–H bonds at 2964 cm^{-1}. Additionally, at 1361 cm^{-1} the bending vibrations of the C–H bonds appeared, while at 1149 cm^{-1}, 1076 cm^{-1}, and 1002 cm^{-1} it is possible to observe the bands of the O–H bending vibration, the C–*O*–C vibration of the glycoside bond and the C–O stretching vibration of the alcohol groups, respectively. The peculiar band at 1646 cm^{-1} is due to the water that is present in the starch because of its hygroscopic properties [42]. Sodium alginate exhibited the same bands as the chitosan and the starch at 3330 cm^{-1}, 2964 cm^{-1}, and 1002 cm^{-1}. Moreover, it presented two bands, corresponding to asymmetrical and symmetric vibrations, associated with the carboxylate anion, at 1600 cm^{-1} and 1405 cm^{-1}, respectively [43]. For the triazene, its spectrum was in accordance with the literature [44] and it was possible to confirm its presence by the bands at 3330 cm^{-1} belonging to the N–H of the triazene.

When comparing the spectrums of the coated samples with the spectrum of pristine PDMS although identical bands are present, coated samples show two additional bands, at 3330 cm^{-1} and 1600 cm^{-1}. By comparing it with the spectra of the individual components, the band at 1600 cm^{-1} belongs to the alginate (i.e., carboxylate anion) while the band at 3330 cm^{-1} may be from all added polymers.

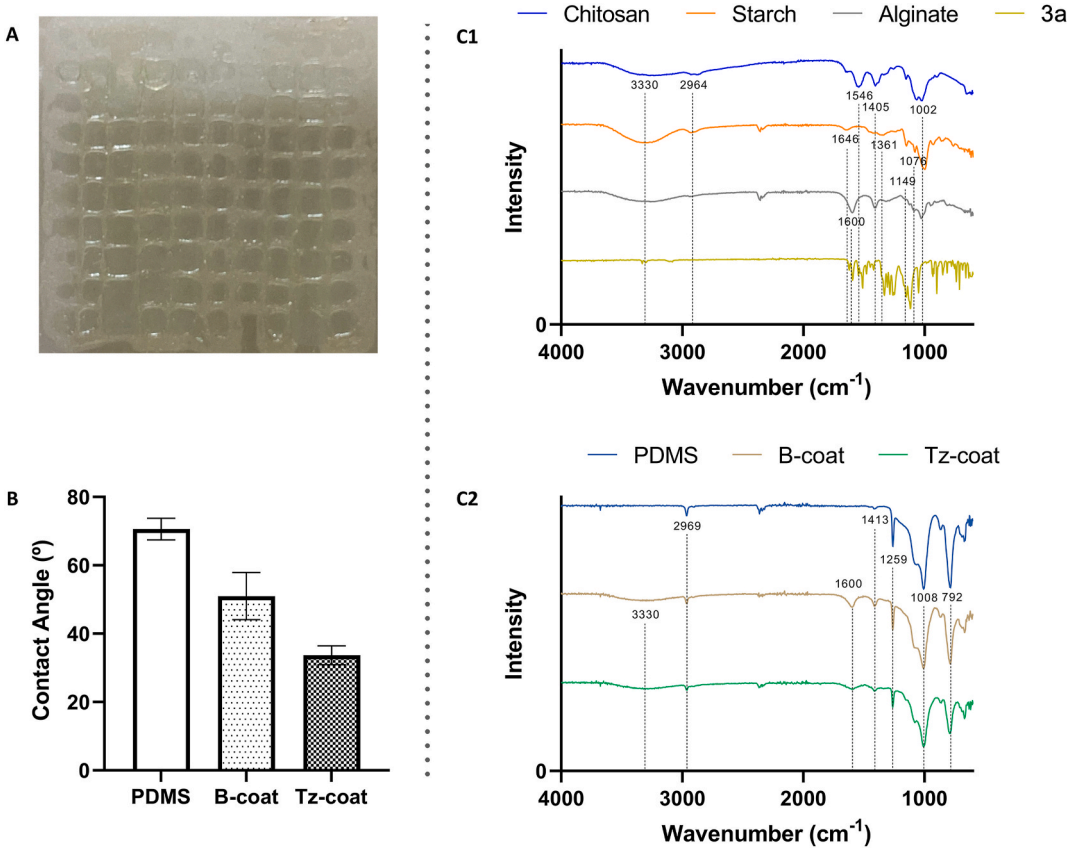

Fig. 4. A. 3D-printed coating comprising a chitosan-starch porous structure loaded with alginate-compound **3a** hydrogel. **B.** Water contact angle obtained for each PDMS segment (with and without coating) 5 min after drop deposition. **C.** FTIR-ATR spectra of materials used for coatings production (i.e., chitosan, starch, sodium alginate, compound **3a**) (**C_1**), and of the PDMS coated segments (B-coat, Tz-coat) and non-coated PDMS (**C_2**).

The scanning electronic microscopy was used to study the coating morphology, chemical composition, and roughness. The non-coated PDMS and PDMS modified with B-coat and Tz-coat are compared in Fig. 5. The SEM image of non-coated PDMS (Fig. 5A_1 and 5A_2) shows large plate-like structures with a length ranging from ~25 to 50 μm (Fig. 5) characteristic from the commercial PDMS used. The roughness and the thickness of these plate-like structures on the PDMS surface was determined through profilogram results (Fig. 5A_3, Fig. 5A_5 and Fig. 5A_6 respectively), revealing a value close to ~4 μm. The EDS analysis of the plate-like structures on PDMS surface (Fig. 5 A4) indicates the presence of nitrogen (N), oxygen (O), carbon (C), magnesium (Mg), and silicon (Si) in composition. The atomic percentages of the N, O, C, Mg and Si are reported in the table inserted in Fig. 5 A_4.

The presence of B-coat on the PDMS surface is evident in SEM images (Fig. 5B_1 and 5B_2) and 3D topographical images (Fig. 5B_3 and 5B_5) where a flatter surface is observed on top of plate-like structures with no

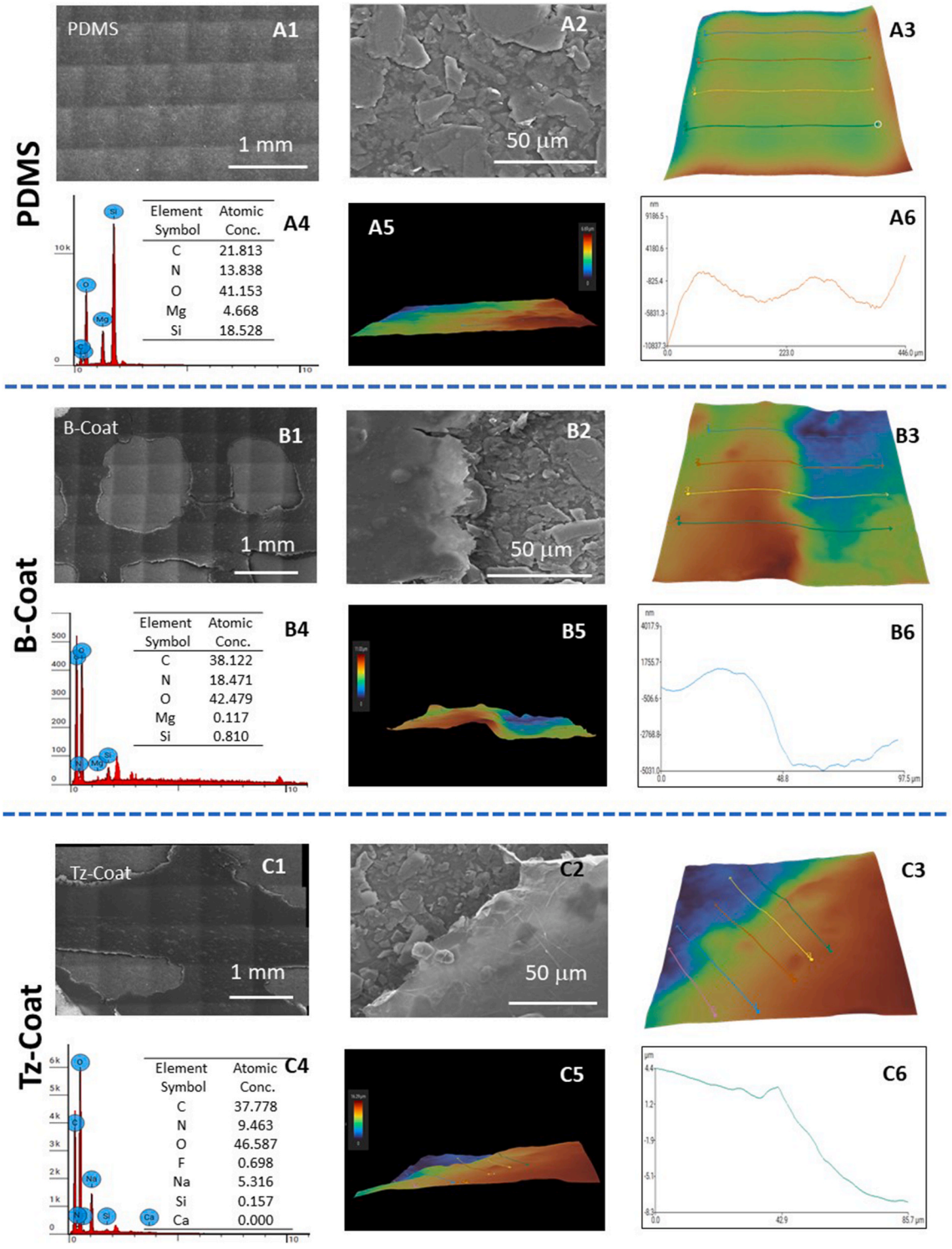

Fig. 5. Morphology, chemical composition, and roughness of coated and uncoated samples. SEM images (A_1, A_2, B_1, B_2, C_1, C_2), 3D topographical images (A_3, A_5, A_6, B_3, B_5, B_6, C_3, C_5, C_6) and EDS analysis (A_4, B_4, C_4) of non-coated PDMS and PDMS coated segments (B-coat, Tz-coat) respectively.

discernible pores. Dual-scale regions on the surface are identified in the 3D topographical images, with the coated area appearing in red and the uncoated area in blue (Fig. 5B_3 and 5B_5). Notably, the thinness of this coating is confirmed by the profilogram plot (Fig. 5B_6), indicating a thickness of approximately 6.5 μm. Moreover, EDS analysis (Fig. 5B_4) reveals no additional elements on the B-coat PDMS surface when compared to PDMS without coating.

Examining the SEM images of Tz-coat PDMS shown in Fig. 5C_1 and C_2, it is confirmed that there is a uniform layer of as-deposited Tz coating on top of the PDMS, displaying large holes (~1 mm in size) characteristics of the design defined in 3D printing process. Additionally, it was found that the morphology of the Tz-coat is quite similar to that of the B-coat.

Considering the 3D topographical images of Tz-coat PDMS (Fig. 5C_3 and C_5), show the same dual-scale regions as observed in B-coat PDMS (Fig. 5B_3 and 5B_5). However, the thickness of the Tz coating (~11 μm) is higher than that of the B-coat (Fig. 5B_6). Additionally, EDS results shown in the table inserted in Fig. 5C_4 reveal the presence of Fluoride (F) and sodium (Na) elements in the Tz coating in addition to those already detected in the PDMS. This suggests the successful integration of Tz into the coating, consistent with the results obtained from FTIR analysis. Moreover, the achieved results revealed that surfaces coated with B-coat and Tz-coat exhibited smoothness in contrast to the rough surface of PDMS.

3.6. Release assay

In Fig. 6A it is possible to observe the release profile of the triazene **3a** from the Tz-coat in an isotonic saline solution at 37 °C, mimicking the physiological conditions. Each coating contained 16 μg of triazene incorporated into the alginate, corresponding to a maximum concentration of triazene **3a** release of 8 μg/mL. The release profile is characterized by a two-step pattern, a fast release till 30 min, reaching a cumulative concentration of 4.0 μg/mL (50 %), followed by a plateau at around 2 h with a final cumulative release of 6.4 μg/mL (80 %) after 72 h. Interestingly, within the first 15 min of the assay, the coating released 1.8 μg/mL of compound **3a**, which is above the MIC for *S. aureus* and close to the MBC (Table 1). This low waiting time for activation ensures rapid action against hazardous microorganisms present in the medium. Overall, the release profile confirms that the novel 3D-printed coating had a suitable microporous structure to provide localized triazene **3a** delivery.

3.7. Biological activity

The antimicrobial susceptibility towards the fabricated coatings was assessed against *S. aureus* by measuring the zone of inhibition formed by coated PDMS segments (i.e., Tz-coat and B-coat). As can be seen in Fig. 6B_1 the Tz-coat showed an inhibition zone of 17.4 ± 0.3 mm (Fig. 6B_2). This shows that compound **3a** was able to diffuse from the coating to the solid medium and inhibit bacteria growth. The levofloxacin control used validated the performed assay since inhibition halos ranging from 25 to 30 mm are described for the inhibition of this bacterial strain [27].

Regarding the antibiofilm activity of PDMS-coated segments against *S. aureus* biofilm, the results can be observed in Fig. 6C. In this assessment, B-coat did not diminish the formation of biofilm of *S. aureus*. This was not expected considering the antimicrobial activity of chitosan previously described in the literature [21]. Maybe the inclusion of alginate gel into the pores leads to the covering of part of chitosan films blocking its activity [26]. On the contrary, the Tz-coat diminished the formation of biofilm by 96 % when compared to the control. This can be explained by the possibility that the bacteria could not proliferate or were even killed by the release of compound **3a** to the medium, as shown in the release assays. Moreover, the rise in wettability observed in contact angle measurements in Tz-coat may also lead to a reduction in *S. aureus* adhesion [25]. Thus, this triazene (**3a**), demonstrated its ability as an antibacterial agent, and when included in a drug release strategy (hydrogel coating), showed potential against *S. aureus* by decreasing surface colonization. Moreover, these 3D-printed coatings seem to show potential for the prevention of medical devices surface colonization and thus medical device-related infections.

As in the previous cytotoxicity tests performed on the compound **3a**, the coatings herein produced were also tested for biocompatibility with HaCat cells. The results were assessed during a 72-h period, with PI and MTT measurements after 24, 48, and 72 h, for measuring membrane integrity and metabolic viability, respectively. According to the release assay during this period the coatings released approximately 6.4 μg/mL to the medium, showing that under these conditions the metabolism of HaCat cells (Fig. 6D) was not affected and that no cytotoxicity was observed towards the membrane (Fig. 6E). This agrees with the expected since no cytotoxicity was observed with 100 μM (42.3 μg/mL) in free compound assays (Fig. 3).

With this study, it was expected to show the potential of 1,3-diaryltriazenes as antimicrobials and their capacity to diminish the development of biofilm. Regarding their antibiofilm activity, it appears to be the first study with these compounds assessing this alarming matter. It is also to highlight the use of 3D printing in medical environments in the tentative to diminish medical device-related infections.

4. Conclusion

In summary, the herein presented work demonstrated the production of a 3D-printed chitosan-starch coating loaded with a 1,3-diaryltriazene derivative alginate hydrogel and its suitability in reducing *S. aureus* growth and biofilm. Relevant chemical synthesis, characterizations, and *in vitro* studies were taken. From the screening of antimicrobial activity, the most suitable synthesized derivative (1,3-bis(4-nitro-2-(trifluoromethyl)phenyl) triazene (**3a**)) was elected for coating incorporation. The resulting three-dimensional gelling structure was achieved to coat a commonly used biomaterial, i.e. medical grade PDMS, leading to an increase in wettability and surface smoothness. The pointed change in the surface properties together with the presence of triazene compound onto the coating can explain the observed antimicrobial effect - led to antimicrobial/antibiofilm activity. A reduction of 96 % on *S. aureus* biofilm was observed which is crucial for reducing biomaterials-related infections. Moreover, the produced coatings showed no cytotoxic effects under the tested conditions.

This study represents a proof of concept illustrating that the combination of a 3D-printing technology and the use of Tz compound can lead to release strategies that reduce biofilm formation on the surface of biomaterials. Moreover, with this work, a new pathway for the use of 1,3-diaryltriazene derivatives was opened concerning the exploration of their antibiofilm activity herein observed for the first time.

CRediT authorship contribution statement

Pedro Vieira: Writing – original draft, Methodology, Investigation, Formal analysis. **Ana F. Bettencourt:** Writing – review & editing, Methodology. **Efthymia Panteli:** Formal analysis. **Catarina Santos:** Writing – original draft, Methodology, Formal analysis. **Lídia M. Gonçalves:** Methodology, Formal analysis. **Ana P. Francisco:** Writing – review & editing, Validation, Supervision, Resources, Conceptualization. **Isabel A.C. Ribeiro:** Writing – review & editing, Validation, Supervision, Resources, Conceptualization.

Declaration of competing interest

The authors declare that they have no known competing financial interests or personal relationships that could have appeared to influence the work reported in this paper.

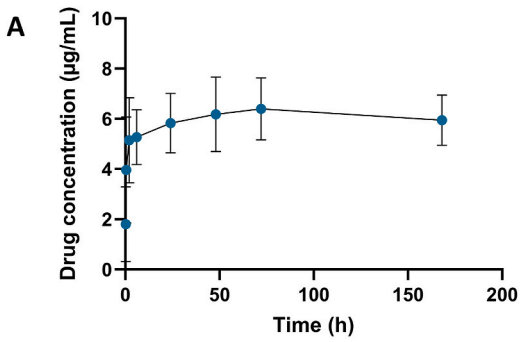

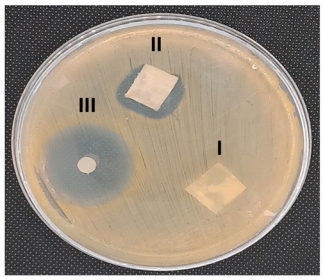

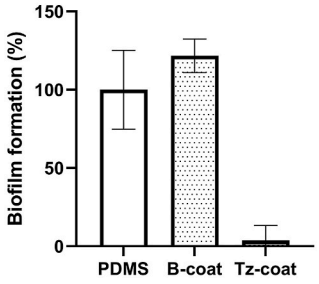

B2

Sample	B-coat (I)	Tz-coat (II)	Levofloxacin (III)
Inhibition (mm)	0	17.4 ± 0.3	29.0 ± 0.2

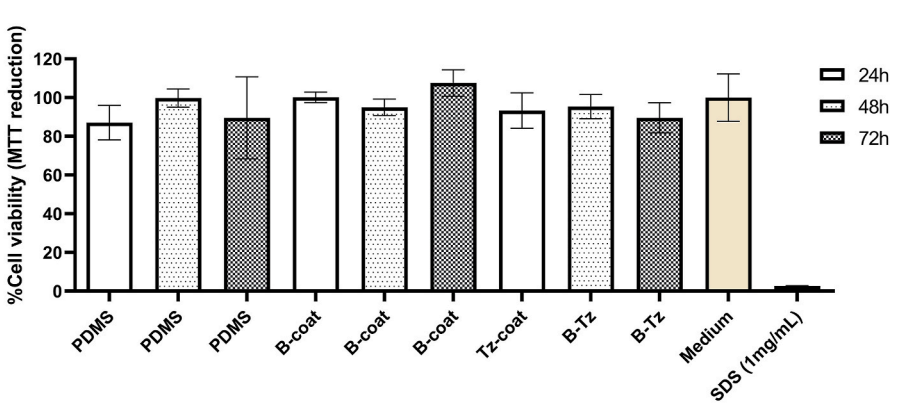

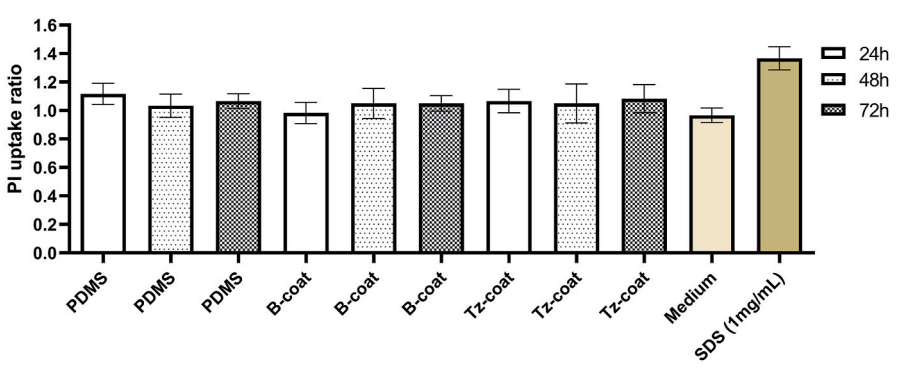

(caption on next page)

Fig. 6. Biological activity of produced coatings. **A.** Release profile of compound **3a** from the Tz-coat expressed in μg/mL, during a 168-h period. **B.** Image (B_1) and values (B_2) of inhibition halos observed with produced coatings ((B-coat (I); Tz-coat (II)) and levofloxacin (III) against *S. aureus*. **C.** Relative biofilm formation of *S. aureus* after 24h of incubation with B-coat and Tz-coat samples. **D.** Relative cell viability of HaCaT cell line determined by the MTT reduction assay after 24h, 48h, and 72h of exposition time to coated and not coated PDMS. **E.** Ratio of PI uptake of HaCaT cells after 24h, 48h, and 72h of exposition time to coated and not coated PDMS.

Data availability

Data will be made available on request.

Acknowledgments

The authors would like to thank the Portuguese government, Fundação para a Ciência e Tecnologia (FCT), for the financial support through national funds: PTDC/BTMSAL/29335/2017; UIDB/04138/2020 and UIDP/04138/2020 through iMED.ULisboa; and UIDB/00100/2020 (https://doi.org/10.54499/UIDB/00100/2020) and LA/P/0056/2020 (https://doi.org/10.54499/LA/P/0056/2020) through Centro de Química Estrutural and of Institute of Molecular Sciences.

Appendix A. Supplementary data

Supplementary data to this article can be found online at https://doi.org/10.1016/j.mtchem.2024.102133.

References

[1] R. Aminov, History of antimicrobial drug discovery: major classes and health impact, Biochem. Pharmacol. 133 (2017) 4–19, https://doi.org/10.1016/J.BCP.2016.10.001.
[2] E. Medina, D.H. Pieper, Tackling threats and future problems of multidrug-resistant bacteria, Curr. Top. Microbiol. Immunol. 398 (2016) 3–33, https://doi.org/10.1007/82_2016_492.
[3] J. Jampilek, Drug repurposing to overcome microbial resistance, Drug Discov. Today 27 (2022) 2028–2041, https://doi.org/10.1016/J.DRUDIS.2022.05.006.
[4] D.B. Kimball, M.M. Haley, Triazenes: a versatile tool in organic synthesis, Angew. Chem. Int. Ed. 41 (2002) 3338–3351, https://doi.org/10.1002/1521-3773(20020916)41:18<3338::AID-ANIE3338>3.0.CO;2-7.
[5] G. Kiefer, T. Riedel, P.J. Dyson, R. Scopelliti, K. Severin, Synthesis of triazenes with nitrous oxide, Angew. Chem. Int. Ed. 54 (2015) 302–305, https://doi.org/10.1002/ANIE.201408597.
[6] S. Bilginer, H.I. Gul, H. Hanci, I. Gulcin, Antibacterial and acetylcholinesterase inhibitory potentials of triazenes containg sulfonamide moiety, Pharm. Chem. J. 55 (2021) 284–289, https://doi.org/10.1007/s11094-021-02412-1.
[7] J. Vajs, C. Proud, A. Brozovic, M. Gazvoda, A. Lloyd, D.I. Roper, M. Osmak, J. Košmrlj, C.G. Dowson, Diaryltriazenes as antibacterial agents against methicillin-resistant Staphylococcus aureus (MRSA) and Mycobacterium smegmatis, Eur. J. Med. Chem. 127 (2017) 223–234, https://doi.org/10.1016/J.EJMECH.2016.12.060.
[8] P. de M.S. Figueirêdo, J.C. Sampaio Filho, A. de J.S. Sodré, J.R. de Castro Júnior, I. S. Gonçalves, R.V. Blasques, R.S. Correa, B.A.V. Lima, L. dos Anjos Marques, D. F. Coutinho, A.P.S. de Azevedo dos Santos, T.R.S.A. Luz, R. de C.M. de Miranda, J. R.A. dos Santos, A.C. Doriguetto, M.I. Pividori, M. Hörner, P.C.M. Villis, Assessment of the biological potential of diaryltriazene-derived triazene compounds, Sci. Rep. 11 (2021) 1–15, https://doi.org/10.1038/s41598-021-81823-2.
[9] A. Al-Azmi, H. Mahmoud, Facile synthesis and antimicrobial activities of novel 1,4-Bis(3,5-dialkyl-4 H-1,2,4-triazol-4-yl)benzene and 5-Aryltriaz-1-en-1-yl-1-phenyl-1 H-pyrazole-4-carbonitrile derivatives, ACS Omega 5 (2020) 10160–10166, https://doi.org/10.1021/acsomega.0c01001.
[10] D. Cappoen, J. Vajs, C. Uythethofken, A. Virag, V. Mathys, M. Kočevar, L. Verschaeve, M. Gazvoda, S. Polanc, K. Huygen, J. Košmrlj, Anti-mycobacterial activity of 1,3-diaryltriazenes, Eur. J. Med. Chem. 77 (2014) 193–203, https://doi.org/10.1016/J.EJMECH.2014.02.065.
[11] P.S. Stewart, T. Bjarnsholt, Risk factors for chronic biofilm-related infection associated with implanted medical devices, Clin. Microbiol. Infection 26 (2020) 1034–1038, https://doi.org/10.1016/j.cmi.2020.02.027.
[12] D. López, H. Vlamakis, R. Kolter, Biofilms, Cold Spring Harb Perspect Biol 2 (2010), https://doi.org/10.1101/CSHPERSPECT.A000398.
[13] H. Pelling, J. Nzakizwanayo, S. Milo, E.L. Denham, W.M. MacFarlane, L.J. Bock, J. M. Sutton, B.V. Jones, Bacterial biofilm formation on indwelling urethral catheters, Lett. Appl. Microbiol. 68 (2019) 277–293, https://doi.org/10.1111/LAM.13144.
[14] Q. Yu, Z. Wu, H. Chen, Dual-function antibacterial surfaces for biomedical applications, Acta Biomater. 16 (2015) 1–13, https://doi.org/10.1016/J.ACTBIO.2015.01.018.
[15] C.M.C. Faustino, S.M.C. Lemos, N. Monge, I.A.C. Ribeiro, A scope at antifouling strategies to prevent catheter-associated infections, Adv. Colloid Interface Sci. 284 (2020) 102–230, https://doi.org/10.1016/J.CIS.2020.102230.
[16] S.I.C. Ricardo, I.I.L. Anjos, N. Monge, C.M.C. Faustino, I.A.C. Ribeiro, A glance at antimicrobial strategies to prevent catheter-associated medical infections, ACS Infect. Dis. 6 (2020) 3109–3130, https://doi.org/10.1021/acsinfecdis.0c00526.
[17] A. Bandyopadhyay, S. Bose, S. Das, 3D printing of biomaterials, MRS Bull. 40 (2015) 108–114, https://doi.org/10.1557/mrs.2015.3.
[18] F. Kong, N. Mehwish, X. Niu, M. Lin, X. Rong, F. Hu, B.H. Lee, Personalized hydrogels for individual health care: preparation, features, and applications in tissue engineering, Mater. Today Chem. 22 (2021) 100612, https://doi.org/10.1016/J.MTCHEM.2021.100612.
[19] S. Zu, Z. Wang, S. Zhang, Y. Guo, C. Chen, Q. Zhang, T. Liu, Q. Liu, Z. Zhang, A bioinspired 4D printed hydrogel capsule for smart controlled drug release, Mater. Today Chem. 24 (2022) 100789, https://doi.org/10.1016/J.MTCHEM.2022.100789.
[20] C. Mortier, D.C.S. Costa, M.B. Oliveira, H.J. Haugen, S.P. Lyngstadaas, J.J. Blaker, J.F. Mano, Advanced hydrogels based on natural macromolecules: chemical routes to achieve mechanical versatility, Mater. Today Chem. 26 (2022) 101222, https://doi.org/10.1016/J.MTCHEM.2022.101222.
[21] A.D. Gholap, S. Rojekar, H.S. Kapare, N. Vishwakarma, S. Raikwar, A. Garkal, T. A. Mehta, H. Jadhav, M.K. Prajapati, U. Annapure, Chitosan scaffolds: expanding horizons in biomedical applications, Carbohydr. Polym. 323 (2024) 121394, https://doi.org/10.1016/J.CARBPOL.2023.121394.
[22] S. Cardoso, F. Narciso, N. Monge, A. Bettencourt, I.A.C. Ribeiro, Improving chitosan hydrogels printability: a comprehensive study on printing scaffolds for customized drug delivery, Int. J. Mol. Sci. 24 (2023), https://doi.org/10.3390/IJMS24020973.
[23] Q. Wei, J. Zhou, Y. An, M. Li, J. Zhang, S. Yang, Modification, 3D printing process and application of sodium alginate based hydrogels in soft tissue engineering: a review, Int. J. Biol. Macromol. 232 (2023) 123450, https://doi.org/10.1016/J.IJBIOMAC.2023.123450.
[24] A.P. Francisco, E. Mendes, A.R. Santos, M.J. Perry, Anticancer triazenes: from bioprecursors to hybrid molecules, Curr Pharm Des 25 (2019) 1623–1642, https://doi.org/10.2174/1381612825666190617155749.
[25] C. Pontes, M. Alves, C. Santos, M.H. Ribeiro, L. Gonçalves, A.F. Bettencourt, I.A. C. Ribeiro, Can Sophorolipids prevent biofilm formation on silicone catheter tubes? Int J Pharm 513 (2016) 697–708, https://doi.org/10.1016/J.IJPHARM.2016.09.074.
[26] F. Narciso, S. Cardoso, N. Monge, M. Lourenço, V. Martin, N. Duarte, C. Santos, P. Gomes, A. Bettencourt, I.A.C. Ribeiro, 3D-printed biosurfactant-chitosan antibacterial coating for the prevention of silicone-based associated infections, Colloids Surf. B Biointerfaces 230 (2023) 113486, https://doi.org/10.1016/J.COLSURFB.2023.113486.
[27] CLSI: Clinical and Laboratory Standards Institute, CLSI Document M100-S23. Performance Standards for Antimicrobial Susceptibility Testing, 21th Informational Supplement, Wayne, Pa, 2013 n.d.
[28] CLSI, Reference Method for Broth Dilution Antifungal Susceptibility Testing of Yeasts; Approved Standard-Third Edition. CLSI Document M27-A3, Clinical and Laboratory Standards Institute, Wayne, PA, 2008.
[29] R.M. Mendes, A.P. Francisco, F.A. Carvalho, M. Dardouri, B. Costa, A. F. Bettencourt, J. Costa, L. Gonçalves, F. Costa, I.A.C. Ribeiro, S. Fighting, Aureus catheter-related infections with sophorolipids: electing an antiadhesive strategy or a release one? Colloids Surf. B Biointerfaces 208 (2021) 112057 https://doi.org/10.1016/J.COLSURFB.2021.112057.
[30] A. Bettencourt, A. Calado, J. Amaral, F.M. Vale, J.M.T. Rico, J. Monteiro, M. Castro, The influence of vacuum mixing on methylmethacrylate liberation from acrylic cement powder, Int J Pharm 219 (2001) 89–93, https://doi.org/10.1016/S0378-5173(01)00630-5.
[31] C. Severo, I. Anjos, V.G.L. Souza, J.P. Canejo, M.R. Bronze, A.L. Fernando, I. Coelhoso, A.F. Bettencourt, I.A.C. Ribeiro, Development of cranberry extract films for the enhancement of food packaging antimicrobial properties, Food Packag. Shelf Life 28 (2021) 100646, https://doi.org/10.1016/J.FPSL.2021.100646.
[32] J. Fernández, I.A.C. Ribeiro, V. Martin, O.L. Martija, E. Zuza, A.F. Bettencourt, J. R. Sarasua, Release mechanisms of urinary tract antibiotics when mixed with bioabsorbable polyesters, Mater. Sci. Eng., C 93 (2018) 529–538, https://doi.org/10.1016/J.MSEC.2018.08.008.
[33] A. Cadete, L. Figueiredo, R. Lopes, C.C.R. Calado, A.J. Almeida, L.M.D. Gonalves, Development and characterization of a new plasmid delivery system based on chitosan-sodium deoxycholate nanoparticles, Eur. J. Pharmaceut. Sci. 45 (2012) 451–458, https://doi.org/10.1016/J.EJPS.2011.09.018.
[34] D.P. Gaspar, V. Faria, L.M.D. Gonçalves, P. Taboada, C. Remuñán-López, A. J. Almeida, Rifabutin-loaded solid lipid nanoparticles for inhaled antitubercular therapy: physicochemical and in vitro studies, Int J Pharm 497 (2016) 199–209, https://doi.org/10.1016/J.IJPHARM.2015.11.050.
[35] M. Rastegar Khosravi, M. Khonsha, R. Ramazanzadeh, Combined effect of levofloxacin and N-acetylcysteine against Enterococcus faecalis biofilm for regenerative endodontics: an in vitro study, Iran. Endod. J. 14 (2019) 40, https://doi.org/10.22037/IEJ.V14I1.21245.

[36] A.C. Matos, C.F. Marques, R.V. Pinto, I.A.C. Ribeiro, L.M. Gonçalves, M.A. Vaz, J. M.F. Ferreira, A.J. Almeida, A.F. Bettencourt, Novel doped calcium phosphate-PMMA bone cement composites as levofloxacin delivery systems, Int J Pharm 490 (2015) 200–208, https://doi.org/10.1016/J.IJPHARM.2015.05.038.

[37] F. Zheng, S. Wang, W. Hou, Y. Xiao, P. Liu, X. Shi, M. Shen, Comparative study of resazurin reduction and MTT assays for cytocompatibility evaluation of nanofibrous materials, Anal. Methods 11 (2019) 483–489, https://doi.org/10.1039/C8AY02310G.

[38] D. Kulig, A. Zimoch-Korzycka, A. Jarmoluk, Cross-linked alginate/chitosan polyelectrolytes as carrier of active compound and beef color stabilizer, Meat Sci. 123 (2017) 219–228, https://doi.org/10.1016/J.MEATSCI.2016.08.010.

[39] N. Ramlan, S.I. Zubairi, M.Y. Maskat, Response surface optimisation of polydimethylsiloxane (PDMS) on borosilicate glass and stainless steel (SS316) to increase hydrophobicity, Molecules 27 (2022) 3388, https://doi.org/10.3390/MOLECULES27113388.

[40] G. Lawrie, I. Keen, B. Drew, A. Chandler-Temple, L. Rintoul, P. Fredericks, L. Grøndahl, Interactions between alginate and chitosan biopolymers characterized using FTIR and XPS, Biomacromolecules 8 (2007) 2533–2541, https://doi.org/10.1021/bm070014y.

[41] S. Govindan, E.A.K. Nivethaa, R. Saravanan, V. Narayanan, A. Stephen, Synthesis and characterization of chitosan–silver nanocomposite, Appl. Nanosci. 2 (2012) 299–303, https://doi.org/10.1007/s13204-012-0109-5.

[42] C. Pozo, S. Rodríguez-Llamazares, R. Bouza, L. Barral, J. Castaño, N. Müller, I. Restrepo, Study of the structural order of native starch granules using combined FTIR and XRD analysis, J. Polym. Res. 25 (2018) 1–8, https://doi.org/10.1007/s10965-018-1651-y.

[43] S. Safi, M. Morshed, S.A. Hosseini Ravandi, M. Ghiaci, Study of electrospinning of sodium alginate, blended solutions of sodium alginate/poly(vinyl alcohol) and sodium alginate/poly(ethylene oxide), J. Appl. Polym. Sci. 104 (2007) 3245–3255, https://doi.org/10.1002/APP.25696.

[44] T. Čimbora-Zovko, A. Brozovic, I. Piantanida, G. Fritz, A. Virag, B. Alič, V. Majce, M. Kočevar, S. Polanc, M. Osmak, Synthesis and biological evaluation of 4-nitro-substituted 1,3-diaryltriazenes as a novel class of potent antitumor agents, Eur. J. Med. Chem. 46 (2011) 2971–2983, https://doi.org/10.1016/J.EJMECH.2011.04.024.